Dynamic Structural Response and Deformations of Monolayer MoS$_2$ Visualized by Femtosecond Electron Diffraction

Ehren M. Mannebach,[†] Renkai Li,[‡] Karel-Alexander Duerloo,[†] Clara Nyby,[§] Peter Zalden,[∥] Theodore Vecchione,[‡] Friederike Ernst,[∥,⊥,#] Alexander Hume Reid,[∥] Tyler Chase,[∥,⊥] Xiaozhe Shen,[‡] Stephen Weathersby,[‡] Carsten Hast,[‡] Robert Hettel,[‡] Ryan Coffee,[‡] Nick Hartmann,[‡] Alan R. Fry,[‡] Yifei Yu,[∇] Linyou Cao,[∇] Tony F. Heinz,[∥,⊥,#] Evan J. Reed,[†,#] Hermann A. Dürr,[∥] Xijie Wang,[‡] and Aaron M. Lindenberg*,[†,∥,#]

[†]Department of Materials Science and Engineering, Stanford University, Stanford, California 94305, United States

[‡]SLAC National Accelerator Laboratory, Menlo Park, California 94025, United States

[§]Department of Chemistry, Stanford University, Stanford, California 94305, United States

[∥]Stanford Institute for Materials and Energy Sciences, SLAC National Accelerator Laboratory, Menlo Park, California 94025, United States

[⊥]Department of Applied Physics, Stanford University, Stanford, California 94305, United States

[#]PULSE Institute, SLAC National Accelerator Laboratory, Menlo Park, California 94025, United States

[∇]Department of Materials Science and Engineering, North Carolina State University, Raleigh, North Carolina 27695, United States

S *Supporting Information*

ABSTRACT: Two-dimensional materials are subject to intrinsic and dynamic rippling that modulates their optoelectronic and electromechanical properties. Here, we directly visualize the dynamics of these processes within monolayer transition metal dichalcogenide MoS$_2$ using femtosecond electron scattering techniques as a real-time probe with atomic-scale resolution. We show that optical excitation induces large-amplitude in-plane displacements and ultrafast wrinkling of the monolayer on nanometer length-scales, developing on picosecond time-scales. These deformations are associated with several percent peak strains that are fully reversible over tens of millions of cycles. Direct measurements of electron−phonon coupling times and the subsequent interfacial thermal heat flow between the monolayer and substrate are also obtained. These measurements, coupled with first-principles modeling, provide a new understanding of the dynamic structural processes that underlie the functionality of two-dimensional materials and open up new opportunities for ultrafast strain engineering using all-optical methods.

KEYWORDS: 2D materials, ultrafast, MoS$_2$, structural dynamics, electron diffraction
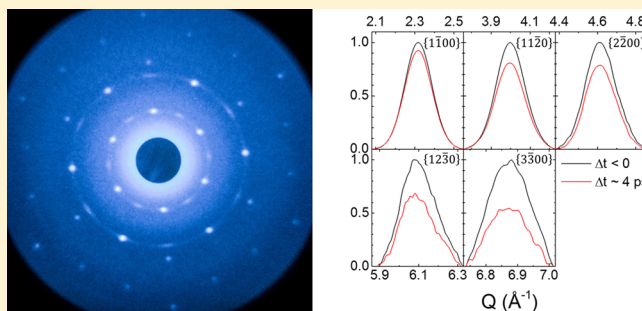
In recent years, there has been tremendous interest in the functional properties of atomically thin transition metal dichalcogenides in the two-dimensional (2D) monolayer limit.[1] Their unique optical and electronic properties[2−4] are intrinsically coupled to their structural properties with strain and interfacial coupling acting as a means to engineer and modulate these responses.[5−9] The ability of quasi-2D materials to withstand large elastic strains has opened up new avenues for controlling their functional properties, including their catalytic properties,[10] band structure,[6,8] and piezoelectric response.[11] However, direct studies of the dynamical structural response of these materials, a key aspect of their functionality, have not been carried out. The strong light-matter coupling exhibited by transition metal dichalcogenides[12,13] in particular points toward novel possibilities for using light to engineer these processes.

Ultrafast optical studies have probed the carrier relaxation and defect scattering dynamics on femtosecond time-scales,[14−18] but these studies are not directly sensitive to lattice degrees of freedom. Previous studies in both graphene and transition metal dichalcogenide monolayers have probed the influence of deformations or wrinkling of the monolayer on its mechanical and electronic degrees of freedom, motivated by potential applications in flexible electronics and as photovoltaic devices.[8,11,19−23] In addition to intrinsic, thermally driven, out-of-plane height fluctuations in the layer thickness,[22] a

buckling transition driven by coupling between in-plane and out-of-plane modes occurs at strain levels of order 0.1−1% in MoS_2 with critical strains sensitive to the number of layers.[24] In the experiments described here, above-gap femtosecond optical excitation leads to large amplitude temperature jumps and compressive in-plane stresses on ultrafast time-scales, and we directly follow the atomic-scale displacements and monolayer rippling in both the in-plane and out-of-plane directions using femtosecond electron scattering as an atomic-scale probe. These temperature jumps and strains are reflected in the time-dependent scattering pattern through both changes in the scattering intensity and through a time-dependent broadening of the diffraction spots, directly encoding the amplitude, orientation, and nanoscale sizes of the ripples. These experiments are enabled by the development of a new source[25] of relativistic (mega-electronvolt) femtosecond electron pulses (see Supporting Information), enabling studies of weakly scattering monolayers with high bunch currents while maintaining short pulse durations, in contrast to existing lower energy sources.[26−29]

Large-area, single-crystal monolayers of MoS_2 were prepared on sapphire substrates from MoO_3 and S source materials in Ar gas and were transferred to a copper TEM grid with a supporting ultrathin amorphous carbon layer (Ted Pella-Quantifoil) via a polystyrene film for electron diffraction measurements in transmission.[30−32] (See the Supporting Information for further details regarding the sample preparation.) A typical diffraction pattern from monolayer 2H-MoS_2 averaged over ~1000 shots (each with a 15 fC charge and 360 fs duration) is shown in Figure 1a and demonstrates the highly crystalline nature of the sample. The sample is dominated by a large, single-crystal domain, as exhibited by the intense six-fold diffraction. There exists a smaller crystal rotated 30° with respect to the main crystal, characteristic of an MoS_2 tilt boundary.[33] All presented data are from analysis of the more intense sets of diffraction peaks. Figure 1b shows the time-dependent response of the diffraction intensity following above-bandgap photoexcitation with 400 nm light (resonant with the C exciton of the MoS_2 crystal) at an incident fluence of ~3.3 mJ/cm^2. Time zero is independently found by measuring the pump-induced deflection in the electron beam associated with a photoemission effect from a gold mesh. Following time zero, we observe an initial decrease in diffracted intensity that turns on in 1.7 ± 0.3 ps (fwhm), reflective of the electron−phonon coupling time in monolayer MoS_2. The time-scales of these effects are significantly slower than our temporal resolution (~0.4 ps), indicating that these processes are likely not driven by nonthermal excitations as observed in other semiconducting materials under similar excitation conditions.[34] This indicates that the electron and lattice systems are equilibrated within ~2 ps. Only data for the first two allowed diffraction peaks ({$1\bar{1}00$} and {$11\bar{2}0$}) of 2H-MoS_2 are shown in Figure 1b for clarity; time scans for all peaks are shown in the Supporting Information, Figure S1. Supporting Information Movie 1 shows the full time-resolved changes of the diffraction pattern. Figure 1c shows snapshots of the diffraction profile for all five measured diffraction peaks comparing before time zero to $\Delta t \sim$ 4 ps after excitation. We observe that the modulation in intensity increases with increasing reciprocal lattice vector **Q**, consistent with a Debye−Waller response, as discussed below. The inset of Figure 1b shows the longer time-scale recovery of the diffraction intensity. We see that the recovery follows a biexponential form with a 53 ± 9 ps time component and a
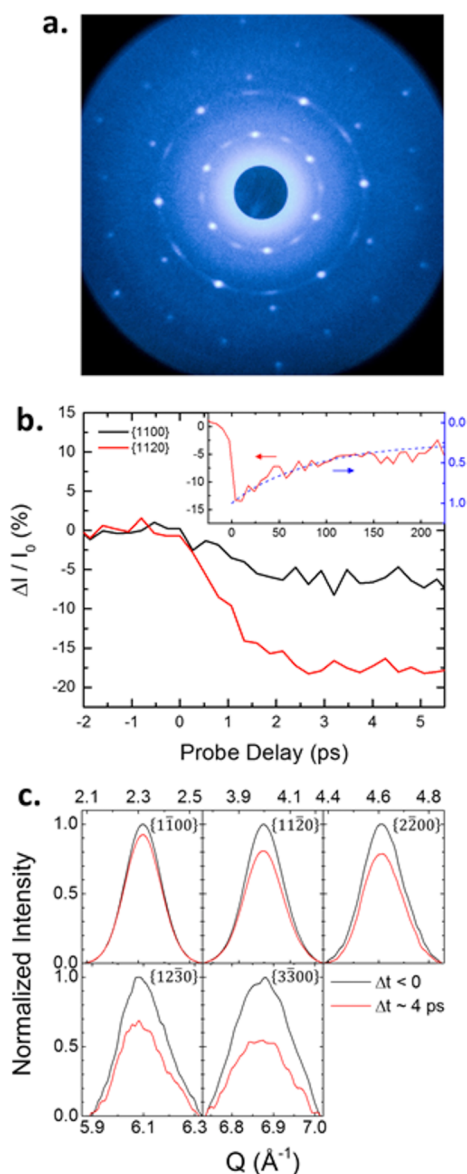

Figure 1. (a) Representative electron diffraction pattern from monolayer MoS_2 (average of 3840 shots). (b) Temporal evolution of the diffraction intensity for two lowest-order diffraction peaks for an incident pump fluence of 3.3 mJ/cm^2. Inset shows the time response at longer probe delays for the {$11\bar{2}0$} peaks overlaid with the COMSOL-simulated MoS_2 temperature (blue dashed line). (c) Experimentally measured (with background subtraction) diffraction profile for all five peaks for the unperturbed sample and after excitation at a delay time of $\Delta t \sim$ 4 ps.

long-lived component. We attribute these time constants to the MoS_2 monolayer transferring heat to the amorphous carbon substrate and to the MoS_2/amorphous carbon system slowly cooling back to ambient temperature via lateral heat flow to unpumped regions of the TEM grid, respectively. The shorter time constant is consistent with COMSOL Multiphysics simulations of MoS_2 monolayer on 20 nm amorphous carbon with a 15 MW m^{-2} K^{-1} thermal boundary resistance between the MoS_2 and the a-C materials (Supporting Information). The inset to Figure 1b also shows an overlay of the long-recovery dynamics with these simulations, showing good agreement. This thermal boundary resistance is roughly consistent with those reported for MoS_2 on other substrates.[35]
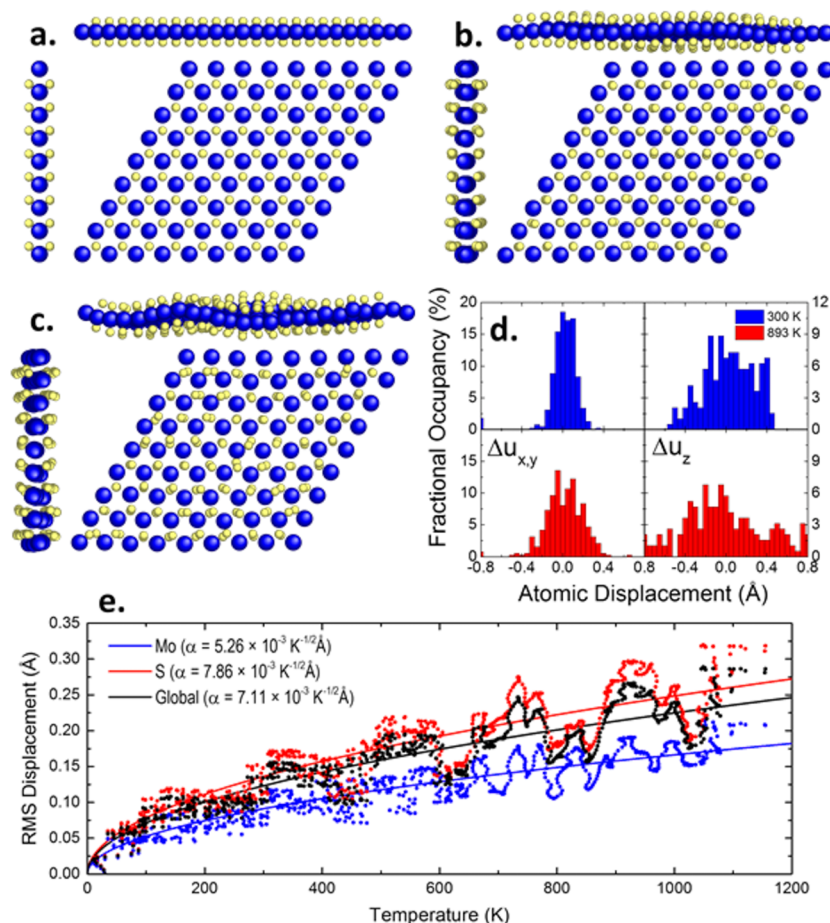
Figure 2. (a−c) Illustration of the ideal MoS$_2$ structure (a) and representative structures at 300 K (b) and 893 K (c), as calculated by molecular dynamics simulations. Side views are along the zigzag (left) and armchair directions (top). (d) Histogram showing the fractional occupation of atomic displacements at a given distance from their equilibrium position. (e) Calculated rms in-plane displacements as a function of lattice temperature. Lines are fits to $\alpha T^{1/2}$.
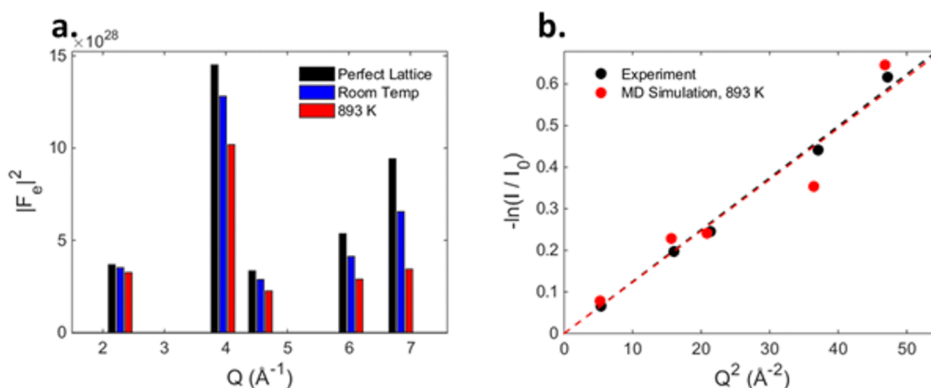

Figure 3. (a) Modulus squared of the MoS$_2$ structure factor calculated from molecular dynamics simulations for the conditions indicated. (b) The Debye−Waller response of MoS$_2$ at a delay of 5 ps after optical excitation. The experimental data are compared to MD simulations. The slope of the linear fit (dashed lines) is half of the pump-induced change in the average in-plane mean square displacement of the atoms, $\Delta\langle u^2 \rangle$. For the simulation data, the values of $|F_e|^2$ from (a) for 300 and 893 K were used as I_0 and I, respectively.

We compare the experimental results at $\Delta t \sim 5$ ps to molecular dynamics (MD) simulations performed using density functional theory within the Projector-Augmented Wave (PAW)[36] pseudopotential implementation of the Vienna Ab Initio Simulation Package (VASP),[37,38] shown in Figure 2. A nonadiabatic approach[39−41] in which nonequilibrium electronic effects are explicitly accounted for is likely not necessary for times longer than the electron−phonon coupling time. Further

details about these calculations are given in the Supporting Information. These calculations allow comparison of the measured diffracted intensity changes to those calculated directly from the simulated atomic displacements. Figure 2a−c shows calculated structures of an ideal 2H-MoS$_2$ monolayer and monolayers at 300 and 893 K. Figure 2d shows a histogram of the fractional occupation of atomic displacements about their in-plane and out-of-plane equilibrium positions, and Figure 2e

presents the calculated root mean square (rms) displacements as a function of lattice temperature for both the Mo and S atoms compared to a $T^{1/2}$ fit. There is a clear and large-scale increase in the disorder of the system at higher temperatures, consistent with an induced thermal disordering of the structure. From snapshots of the MD simulations, we directly calculate the structure factor for each measured reflection using the simulated atomic coordinates (Supporting Information). Figure 3a shows how this increase in disorder affects the modulus squared of the structure factor (directly proportional to the diffraction intensity) for MoS_2, where black, blue, and red bars correspond to a perfect MoS_2 lattice, a lattice at 300 K, and a lattice at 893 K, respectively. This shows that the magnitude of the structure factor (i.e., diffraction intensity) decreases with temperature, as expected, with stronger suppression of the diffraction occurring at higher reciprocal lattice vectors. We can quantitatively understand this effect via a Debye−Waller response[42] following $I = I_0 e^{-Q^2 \langle u_Q^2 \rangle}$, where I and I_0 are the pumped and unpumped (300 K for MD simulation) diffraction intensities, $\mathbf{Q}$ is the reciprocal lattice vector of the diffraction peak, and $\langle u_Q^2 \rangle$ is the time-average mean-square displacement of the atoms in the direction of $\mathbf{Q}$. In the transmission geometry relevant for this experiment, only the (0001) zone axis of MoS_2 was probed. This makes the structure factors sensitive only to positions of atoms in the plane of the monolayer, since $\mathbf{Q}$ is always in the monolayer plane. Assuming isotropic in-plane displacements of atoms, as also observed in the MD simulations, we expect that $\langle u_{\text{in-plane}}^2 \rangle = 2\langle u_Q^2 \rangle$ such that we can rewrite the Debye−Waller response purely in terms of the in-plane displacements as $I = I_0 e^{-Q^2 \langle u_{\text{in-plane}}^2 \rangle/2}$, or $-\ln(I/I_0) = Q^2 \langle u_{\text{in-plane}}^2 \rangle /2$. If we fit the data from Figures 1b and 3a to this relationship, we obtain very good agreement (Figure 3b), where the slope of the fit (dashed line) is twice that of the increase in the in-plane mean square displacement of the atoms about their equilibrium position following optical pumping. We note that the rms displacements calculated from the MD simulations are in agreement with the experimentally determined displacements for a simulated temperature jump of ∼600 K. This is roughly consistent with the temperature jump expected based on the known absorbance and heat capacity of MoS_2 (Supporting Information). Figure 4a shows the experimentally determined, time-dependent change in mean square displacement of atoms for the five accessible MoS_2 diffraction peaks using the same equation given above with data from all measured reflections collapsed to a single curve (Figure 4a,b). We see induced changes in the mean square displacement of ∼0.024 Å² in all five accessible reflections, corresponding to an increase in the rms in-plane atomic displacement of ∼0.15 Å. These estimates of the mean square displacements and associated Debye−Waller factor are consistent with simple estimates of the thermally driven displacements at this excitation fluence (Supporting Information).

At a slightly higher pump fluence (4.4 mJ/cm²), we observe photoinduced shifts in Q and a symmetrical broadening of the diffraction peaks occurring on the time-scale of a few picoseconds (Figure 5a). These effects are comparable to the time-scales for the generation of the in-plane displacements and are reversible at the 120 Hz repetition rate of the experiment. The peak broadening can be explained by an induced buckling/rippling of the thin monolayer, previously studied by static electron microscopy techniques.[19,21,43] When the monolayer
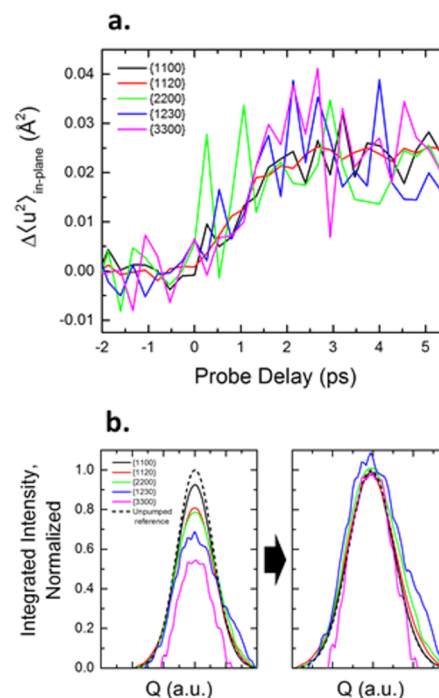
a.

b.

Figure 4. (a) Extracted time response of the in-plane mean squared atomic displacements. Overlap of curves for all reflections indicates consistency with the Debye−Waller model. (b) Lineouts for all measured reflections taken from Figure 1c (left) and scaled by the Debye−Waller factor $e^{-Q^2 \langle u_{\text{in-plane}}^2 \rangle /2}$ (right), which collapses the measured data onto a single curve.

dynamically ripples, the crystal truncation rods from one region of the sample (which are aligned with the monolayer plane normal, Figure 5c) become tilted in reciprocal space in a slightly different direction as compared to those from a different region of the sample, as shown schematically in Figure 5d. This leads to an induced nonzero intensity in cone-shaped regions of reciprocal space, as opposed to sharp rods from a perfectly flat sample. The intersection of these cone-shaped regions in reciprocal space with the (essentially flat) Ewald sphere then manifests as a broadening of the peak width. We note that our sample was aligned normal to the electron propagation direction to an accuracy of $\varphi = 2°$; sample tilts tilt the Ewald sphere and allow for sampling of this broadening of the cone-shaped regions of reciprocal space (Figure 5d, dashed lines). The magnitude of φ sets a lower bound on the magnitude of the pump-induced rippling, with the effective angle of the rippling $\Delta\theta$ given by

$$\Delta\theta = \frac{\Delta\sigma}{\varphi Q} \tag{1}$$

where $\Delta\sigma$ is the broadening of the diffraction spot and Q is the corresponding in-plane momentum transfer for the reflection (Supporting Information Section 4). The broadening of the peak (change in reciprocal space cone angle) is directly related to the angle of the ripples; however, the change in peak width measured in this experiment is a convolution of the intrinsic diffracted electron beam size and the pump-induced broadening of the reciprocal space cones. By subtracting in quadrature the intrinsic electron beam size from the experiment, the experimentally measured broadening of 1.2% for the $\{11\bar{2}0\}$ reflection corresponds to an actual broadening of 15.5%.
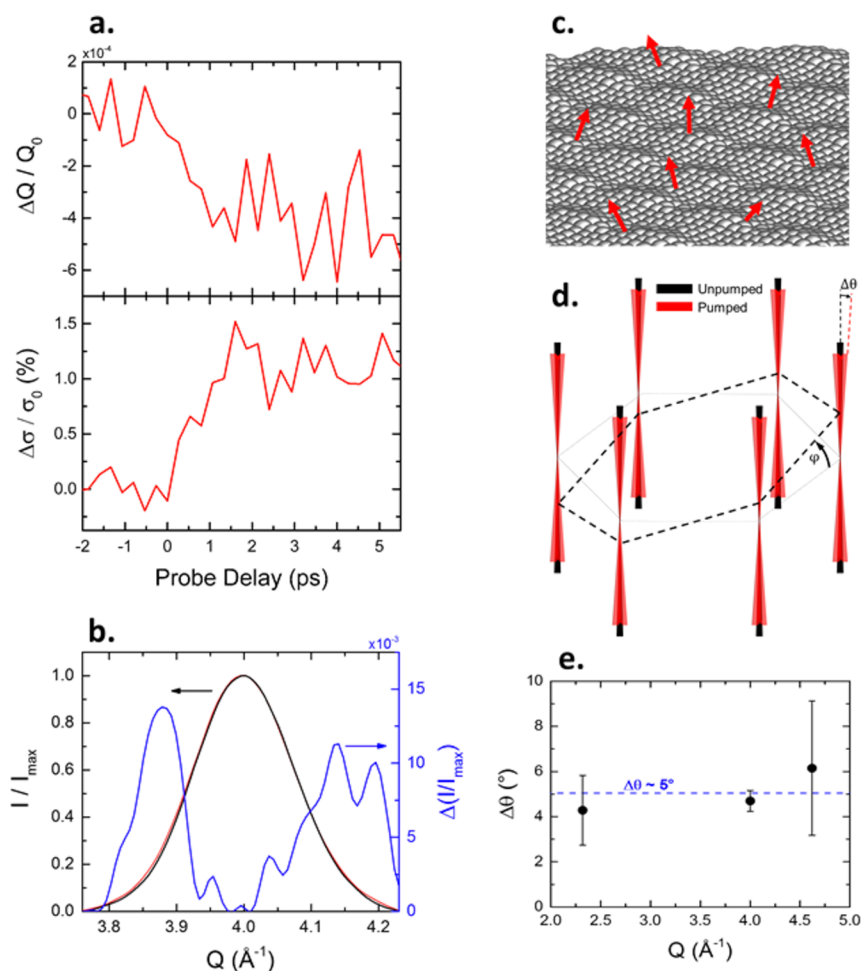
Figure 5. (a) Time-dependent shifts $\Delta Q/Q$ and broadening $\Delta\sigma/\sigma$ for the $\{11\overline{2}0\}$ reflection showing concurrent strains and broadening associated with rippling of the monolayer developing on few picosecond time-scales. (b) Normalized data for the $\{11\overline{2}0\}$ reflection with the shift ΔQ removed, comparing the initial response before optical excitation (black) with the response at a delay time Δt of 4 ps (red), showing broadening effects. The blue curve is the differential intensity $I(\Delta t \sim 4\,\text{ps}) - I(\Delta t < 0)$. (c,d) Diffraction intensities for monolayer MoS_2 are given by sharp rods in reciprocal space parallel to the surface normal. If the monolayer is rippled/buckled, the diffraction intensities are given by a superposition of many rods with slightly different orientation, resulting in a cone-shaped distribution. Optical pumping increases the magnitude of the ripples by an angle $\Delta\theta$, thereby broadening the cone-shaped distribution of diffracted intensity. Slightly tilting the sample by φ tilts the Ewald sphere in reciprocal space (gray dotted line to black dashed line), allowing for measurement of the diffraction peak broadening. (e) Diffraction cone angle calculated from the peak broadening of the $\{1\overline{1}00\}$, $\{1\overline{2}00\}$, and $\{2\overline{2}00\}$ diffraction peaks.

Taking $\varphi = 2°$ the increase in reciprocal space cone angle is 5° (Figure 5e and Supporting Information). This means the local surface normals deviate $\sim2.5°$ from the mean sample surface. These estimates are in agreement with the predicted ripple angles from the MD simulations for a freely suspended monolayer (Figure 2). Analysis for the $\{1\overline{1}00\}$ and $\{2\overline{2}00\}$ reflections gives similar results for $\Delta\theta$ (Figure 5e). From the observed symmetric broadening of the diffraction peaks, we conclude that the ripples are randomly oriented within the probed crystalline domain. An upper limit on the lateral size of the ripples is estimated by the time scale of the associated shifts in Q or the onset of the peak broadening response (~2 ps) multiplied by the in-plane sound velocity of MoS_2, indicating that the lateral ripple size must be less than 10 nm. Assuming a lateral ripple radius of 6 nm (consistent with ref 21 in the static case), we find a maximum pump-induced ripple height of ~1 Å. These observations are roughly consistent with theoretical predictions[44] for the amplitude A of the buckling of a quasi-2D monolayer under strain ε clamped at ends a distance L apart, with $A^2 \sim \nu t L[(16\varepsilon)/(3\pi^2(1-\nu^2))]^{1/2}$ where t is the sample

thickness, and ν is Poisson's ratio. Taking the strain directly from the measured shifts in Q ($\varepsilon \sim \Delta Q/Q \sim 5 \times 10^{-4}$) and taking L to be the size of the ripple as estimated above, this gives an amplitude of ~1 Å, in good agreement with the experimental results. The maximum tensile strain ε_{max} is accumulated at the peak of the induced ripples and can be estimated as[6] $\varepsilon_{max} \sim \pi^2 A t/(1-\nu^2)L^2$. With L as above, this corresponds to a pump-induced peak strain of $\sim2.5\%$. These effects are fully reversible at the 120 Hz repetition rate of the experiment.

The induced rippling can be viewed from two essentially equivalent perspectives. (1) Because the photoexcited region of the sample is ~1 mm^2, the pumped region of the sample is kinetically clamped to its initial dimensions on the time scales of this experiment; that is to say, a coherent lateral thermal expansion is not allowed because the time it takes for the material to expand is far longer than the time scale of the experiment. Instead, the monolayer accommodates the thermal expansion by rippling on nanometer length-scales, associated with excitation of displacements in the out-of-plane direction.

Taking typical values for the elastic modulus and the thermal expansion coefficient, we estimate an in-plane stress of ∼1 GPa under these excitation conditions. (2) Alternatively, these ripples can be viewed as directly driven by thermal fluctuations, following an ultrafast temperature jump with the underlying substrate only allowing large amplitude displacements perpendicular to the plane of the sample. As expected, the magnitude of the measured photoinduced shifts $\Delta Q/Q$ is comparable to what we would expect for the associated induced temperature jumps assuming known values for the thermal expansion coefficient.

In summary, we show that photoexcitation of monolayer MoS_2 films gives rise to large-amplitude in-plane atomic displacements and out-of-plane wrinkling with percent-level peak strains. Because these films exhibit abilities to withstand giant strains and intense photoexcitation conditions in a reversible fashion,[14] new possibilities for all-optical dynamic control of wrinkling degrees of freedom and their coupled electronic and optical responses follow from this work. For example, the peak strains extracted above correspond to spatially inhomogeneous modulations in the band gap of ∼0.1 eV[6] and present novel opportunities for tuning the band structure with light on picosecond time-scales. The sample studied in this work showed stability over tens of millions of shots. Future studies on freely suspended films and complex 2D layered material heterostructures can be carried out using similar techniques. The pump−probe techniques described here allow for studies of small, thermally induced structural changes under quasi-equilibrium conditions, difficult to resolve with static heating approaches, including direct measurements of thermal boundary resistances across buried interfaces. Finally, new possibilities for directly probing dynamic fluctuations through inelastic scattering as reflected in the time-dependent diffuse scattering pattern will open up new windows into the phenomena observed here.

■ ASSOCIATED CONTENT

ⓢ Supporting Information

The Supporting Information is available free of charge on the ACS Publications website at DOI: 10.1021/acs.nanolett.5b02805.

> Time response of all observed diffraction peaks, calculation of structure factor from MD simulations, optical pump-induced thermal effects, calculation of ripple angle from diffraction peak broadening, and details about the experimental methods. (PDF)
> Movie showing the full time-resolved changes of the diffraction pattern. (ZIP)

■ AUTHOR INFORMATION

Corresponding Author
*E-mail: aaronl@stanford.edu.

Author Contributions
The manuscript was written through contributions of all authors. All authors have given approval to the final version of the manuscript. E.M., R.L, C.N., T.V., A.R., T.C., X.S., S.W, X.W., and A.L. carried out the experiments. K.D. and E.R. carried out the molecular dynamics simulations. P.Z. carried out the thermal diffraction and transport simulations. F.E., Y.Y., and L.C. led the sample synthesis efforts. R.C., N.H., and A.F. led the laser development efforts. X.W., R.H., C.H., and H.D. led
the development of the UED source. The experiment was conceived by A.L.

■ ABBREVIATIONS
TEM, transmission electron microscope; fwhm, full-width at half-maximum; MD, molecular dynamics; PAW, projector-augmented wave; VASP, Vienna ab initio simulation package; UED, ultrafast electron diffraction

■ REFERENCES
(1) Service, R. *Science* **2015**, *348*, 490−492.
(2) Mak, K.; Lee, C.; Hone, J.; Shan, J.; Heinz, T. *Phys. Rev. Lett.* **2010**, *105*, 136805.
(3) Seyler, K. L.; Schaibley, J. R.; Gong, P.; Rivera, P.; Jones, A. M.; Wu, S.; Yan, J.; Mandrus, D. G.; Yao, W.; Xu, X. *Nat. Nanotechnol.* **2015**, *10*, 407.
(4) Butler, S. Z.; Hollen, S. M.; Cao, L.; Cui, Y.; Gupta, J. A.; Gutiérrez, H. R.; Heinz, T. F.; Hong, S. S.; Huang, J.; Ismach, A. F.; Johnston-Halperin, E.; Kuno, M.; Plashnitsa, V. V.; Robinson, R. D.; Ruoff, R. S.; Salahuddin, S.; Shan, J.; Shi, L.; Spencer, M. G.; Terrones, M.; Windl, W.; Goldberger, J. E. *ACS Nano* **2013**, *7*, 2898−2926.
(5) Duerloo, K. N.; Li, Y.; Reed, E. J. *Nat. Commun.* **2014**, *5*, 4214.
(6) Castellanos-Gomez, A.; Roldán, R.; Cappelluti, E.; Buscema, M.; Guinea, F.; van der Zant, H. S. J.; Steele, G. A. *Nano Lett.* **2013**, *13*, 5361−5366.
(7) Conley, H. J.; Wang, B.; Ziegler, J. I.; Haglund, R. F., Jr.; Pantelides, S. T.; Bolotin, K. I. *Nano Lett.* **2013**, *13*, 3626−3630.
(8) Feng, J.; Qian, X.; Huang, C.-W.; Li, J. *Nat. Photonics* **2012**, *6*, 866−872.
(9) Duerloo, K.-A. N.; Ong, M. T.; Reed, E. J. *J. Phys. Chem. Lett.* **2012**, *3*, 2871−2876.
(10) Voiry, D.; Yamaguchi, H.; Li, J.; Silva, R.; Alves, D. C. B.; Fujita, T.; Chen, M.; Asefa, T.; Shenoy, V. B.; Eda, G.; Chhowalla, M. *Nat. Mater.* **2013**, *12*, 850−855.
(11) Duerloo, K.-A. N.; Reed, E. J. *Nano Lett.* **2013**, *13*, 1681−1686.
(12) Bernardi, M.; Palummo, M.; Grossman, J. C. *Nano Lett.* **2013**, *13*, 3664−3670.
(13) Li, Y.; Chernikov, A.; Zhang, X.; Rigosi, A.; Hill, H. M.; van der Zande, A. M.; Chenet, D. A.; Shih, E.-M.; Hone, J.; Heinz, T. F. *Phys. Rev. B: Condens. Matter Mater. Phys.* **2014**, *90*, 205422−205426.
(14) Mannebach, E. M.; Duerloo, K.-A. N.; Pellouchoud, L. A.; Sher, M.-J.; Nah, S.; Kuo, Y.-H.; Yu, Y.; Marshall, A. F.; Cao, L.; Reed, E. J.; Lindenberg, A. M. *ACS Nano* **2014**, *8*, 10734−10742.
(15) Shi, H.; Yan, R.; Bertolazzi, S.; Brivio, J.; Gao, B.; Kis, A.; Jena, D.; Xing, H. G.; Huang, L. *ACS Nano* **2013**, *7*, 1072−1080.
(16) Kumar, N.; Cui, Q.; Ceballos, F.; He, D.; Wang, Y.; Zhao, H. *Phys. Rev. B: Condens. Matter Mater. Phys.* **2014**, *89*, 125427.
(17) Wang, R.; Ruzicka, B.; Kumar, N.; Bellus, M.; Chiu, H.-Y.; Zhao, H. *Phys. Rev. B: Condens. Matter Mater. Phys.* **2012**, *86*, 045406.
(18) Sun, D.; Rao, Y.; Reider, G. A.; Chen, G.; You, Y.; Brézin, L.; Harutyunyan, A. R.; Heinz, T. F. *Nano Lett.* **2014**, *14*, 5625−5629.
(19) Meyer, J. C.; Geim, A. K.; Katsnelson, M. I.; Novoselov, K. S.; Booth, T. J.; Roth, S. *Nature* **2007**, *446*, 60−63.
(20) Mermin, N. D. *Phys. Rev.* **1968**, *176*, 250.

(21) Brivio, J.; Alexander, D. T. L.; Kis, A. *Nano Lett.* **2011**, *11*, 5148−5153.

(22) Miró, P.; Ghorbani-Asl, M.; Heine, T. *Adv. Mater.* **2013**, *25*, 5473−5475.

(23) Zang, J.; Ryu, S.; Pugno, N.; Wang, Q.; Tu, Q.; Buehler, M. J. *Nat. Mater.* **2013**, *12*, 321−325.

(24) Singh, S. K.; Neek-Amal, M.; Costamagna, S.; Peeters, F. M. *Phys. Rev. B: Condens. Matter Mater. Phys.* **2015**, *91*, 014101−014107.

(25) Weathersby, S. P.; Brown, G.; Centurion, M.; Chase, T. F.; Coffee, R.; Corbett, J.; Eichner, J. P.; Frisch, J. C.; Fry, A. R.; Gühr, M.; Hartmann, N.; Hast, C.; Hettel, R.; Jobe, R. K.; Jongewaard, E. N.; Lewandowski, J. R.; Li, R. K.; Lindenberg, A. M.; Makasyuk, I.; May, J. E.; McCormick, D.; Nguyen, M. N.; Reid, A. H.; Shen, X.; Sokolowski-Tinten, K.; Vecchione, T.; Vetter, S. L.; Wu, J.; Yang, J.; Dürr, H. A.; Wang, X. J. *Rev. Sci. Instrum.* **2015**, *86*, 073702−073707.

(26) Gulde, M.; Schweda, S.; Storeck, G.; Maiti, M.; Yu, H.; Wodtke, A.; Schafer, S.; Ropers, C. *Science* **2014**, *345*, 200.

(27) Zewail, A. *Annu. Rev. Phys. Chem.* **2006**, *57*, 65.

(28) Sciaini, G.; Miller, R. J. D. *Rep. Prog. Phys.* **2011**, *74*, 096101.

(29) Hastings, J. B.; Rudakov, F. M.; Dowell, D. H.; Schmerge, J. F.; Cardoza, J. D.; Castro, J. M.; Gierman, S. M.; Loos, H.; Weber, P. M. *Appl. Phys. Lett.* **2006**, *89*, 184109−4.

(30) Yu, Y.; Li, C.; Liu, Y.; Su, L.; Zhang, Y.; Cao, L. *Sci. Rep.* **2013**, *3*, 1866.

(31) Lee, Y.-H.; Zhang, X.-Q.; Zhang, W.; Chang, M.-T.; Lin, C.-T.; Chang, K.-D.; Yu, Y.-C.; Wang, J. T.-W.; Chang, C.-S.; Li, L.-J.; Lin, T.-W. *Adv. Mater.* **2012**, *24*, 2320−2325.

(32) Gurarslan, A.; Yu, Y.; Su, L.; Yu, Y.; Suarez, F.; Yao, S.; Zhu, Y.; Ozturk, M.; Zhang, Y.; Cao, L. *ACS Nano* **2014**, *8*, 11522−11528.

(33) Najmaei, S.; Liu, Z.; Zhou, W.; Zou, X.; Shi, G.; Lei, S. *Nat. Mater.* **2013**, *12*, 754−759.

(34) Lindenberg, A. M.; Larsson, J.; Sokolowski-Tinten, K.; Gaffney, K. J.; Blome, C.; Synnergren, O.; Sheppard, J.; Caleman, C.; MacPhee, A. G.; Weinstein, D.; Lowney, D. P.; Allison, T.; Matthews, T.; Falcone, R.; Cavalieri, A.; Fritz, D. M.; Lee, S. H.; Bucksbaum, P. H.; Reis, D. A.; Rudati, J.; Fuoss, P. H.; Kao, C. C.; Siddons, D. P.; Pahl, R.; Als-Nielsen, J.; Duesterer, S.; Ischebeck, R.; Schlarb, H.; Schulte-Schrepping, H.; Tschentscher, T.; Schneider, A.; Linde; Von der, D.; Hignette, O.; Sette, F.; Chapman, H. N.; Lee, R. W.; Hansen, T. N.; Techert, S.; Wark, J. S.; Bergh, M.; Huldt, G.; van der Spoel, D.; Timneanu, N.; Hajdu, J.; Akre, R. A.; Bong, E.; Krejcik, P.; Arthur, J.; Brennan, S.; Luening, K.; Hastings, J. B. *Science* **2005**, *308*, 392−395.

(35) Taube, A.; Judek, J.; Łapińska, A. *ACS Appl. Mater. Interfaces* **2015**, *7*, 5061.

(36) Kresse, G.; Joubert, D. *Phys. Rev. B: Condens. Matter Mater. Phys.* **1999**, *59*, 1758−1775.

(37) Perdew, J. P.; Burke, K.; Ernzerhof, M. *Phys. Rev. Lett.* **1996**, *77*, 3865−3868.

(38) Kresse, G.; Furthmüller, J. *Phys. Rev. B: Condens. Matter Mater. Phys.* **1996**, *54*, 11169−11186.

(39) Nelson, T.; Fernandez-Alberti, S.; Roitberg, A. E.; Tretiak, S. *Acc. Chem. Res.* **2014**, *47*, 1155−1164.

(40) Tully, J. C. *J. Chem. Phys.* **1990**, *93*, 1061.

(41) Craig, C. F.; Duncan, W. R.; Prezhdo, O. V. *Phys. Rev. Lett.* **2005**, *95*, 163001−163004.

(42) Singh, N.; Sharma, P. K. *Phys. Rev. B* **1971**, *3*, 1141−1148.

(43) Meyer, J. C.; Geim, A. K.; Katsnelson, M. I.; Novoselov, K. S.; Obergfell, D.; Roth, S.; Girit, C.; Zettl, A. *Solid State Commun.* **2007**, *143*, 101−109.

(44) Bao, W.; Miao, F.; Chen, Z.; Zhang, H.; Jang, W.; Dames, C.; Lau, C. N. *Nat. Nanotechnol.* **2009**, *4*, 562−566.